STRUCTURAL CHEMISTRY

ISSN 2053-2296

Fe^{III} in the high-spin state in dimethylammonium bis[3-ethoxysalicylaldehyde thiosemicarbazonato(2−)-κ^3O^2,N^1,S]ferrate(III)

Robyn E. Powell,[a] Martin R. Lees,[b] Graham J. Tizzard,[c] Simon J. Coles,[c] Qingchun Yuan[d] and Petra J. van Koningsbruggen[a]*

[a]College of Engineering and Physical Sciences, School of Infrastructure and Sustainable Engineering, Department of Chemical Engineering and Applied Chemistry, Aston University, Aston Triangle, Birmingham, West Midlands, B4 7ET, United Kingdom, [b]Department of Physics, University of Warwick, Coventry, CV4 7AL, United Kingdom, [c]National Crystallography Service, Chemistry, University of Southampton, Southampton, SO17 1BJ, United Kingdom, and [d]Energy and Bioproducts Research Institute, College of Engineering and Physical Sciences, Aston University, Birmingham, B4 7ET, United Kingdom. *Correspondence e-mail: p.vankoningsbruggen@aston.ac.uk

Received 7 November 2022
Accepted 1 December 2022

Edited by D. R. Turner, University of Monash, Australia

Keywords: Fe^{III} complex; high-spin; crystal structure; thiosemicarbazone; salicylaldehyde; magnetic susceptibility.

CCDC reference: 2223775

Supporting information: this article has supporting information at journals.iucr.org/c

The synthesis and crystal structure (100 K) of the title compound, $[(CH_3)_2NH_2][Fe(C_{10}H_{11}O_2N_3S)_2]$, are reported. The asymmetric unit consists of an octahedral $[Fe^{III}(L)_2]^-$ fragment, where L^{2-} is 3-ethoxysalicylaldehyde thiosemicarbazonate(2−), and a dimethylammonium cation. Each L^{2-} ligand binds with the thiolate S, the imine N and the phenolate O atoms as donors, resulting in an $Fe^{III}S_2N_2O_2$ chromophore. The ligands are orientated in two perpendicular planes, with the O and S atoms in *cis* positions, and mutually *trans* N atoms. The Fe^{III} ion is in the high-spin state at 100 K. The variable-temperature magnetic susceptibility measurements (5–320 K) are consistent with the presence of a high-spin Fe^{III} ion with D = 0.83 (1) cm^{-1} and g = 2.

1. Introduction

The continuing research and development of switchable magnetic, optical and/or photomagnetic materials seeks to provide solutions for the societal desire towards more advanced electronic devices (*e.g.* larger data storage capacity and faster data processing) and their miniaturization by offering industry novel magnetic materials that can be implemented in electronic devices for information storage and as displays (Létard *et al.*, 2004; Gütlich *et al.*, 2004; Gütlich & Goodwin, 2004; van Koningsbruggen *et al.* 2004; Halcrow, 2013; Molnár *et al.*, 2018; Senthil Kumar *et al.*, 2017; Rubio-Giménez *et al.*, 2019; Tissot *et al.*, 2019; Karuppannan *et al.*, 2021). Spin-crossover materials have attractive physical properties that make them suitable candidates for fulfilling these requirements. Such compounds exhibiting a temperature-dependent crossover between electronic states having a different magnetic moment were first discovered for iron(III) tris(dithiocarbamates) (Cambi & Szegö, 1931, 1933). Since then, two main families of Fe^{III} spin-crossover systems have been extensively studied, *i.e.* those containing ligands sporting chalcogen donor atoms and those based on multidentate *N*,*O*-donating Schiff base-type ligands (van Koningsbruggen *et al.*, 2004; Harding *et al.*, 2016). It has been found that the magnetic interconversion between the low-spin (S = 1/2) and high-spin (S = 5/2) state in Fe^{III} systems can be triggered by a change in temperature or pressure, or by light irradiation (Hayami *et al.*, 2000, 2009; van Koningsbruggen *et al.*, 2004; Harding *et al.*, 2016).

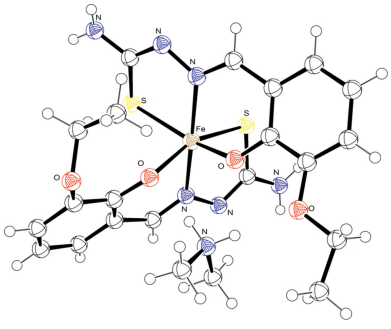

The generation of Fe^{III} spin-crossover behaviour using particular salicylaldehyde thiosemicarbazone derivatives has been extensively studied by several research groups (van Koningsbruggen *et al.*, 2004; Phonsri *et al.*, 2017; Powell *et al.*, 2014, 2015, 2020, 2022; Powell, 2016; Yemeli Tido, 2010; Zelentsov *et al.*, 1973; Ryabova *et al.*, 1978, 1981*a*,*b*, 1982; Floquet *et al.*, 2003, 2006, 2009; Li *et al.*, 2013, 2016).

Our research demonstrated that the electronic state of an Fe^{III} ion surrounded by two such tridentate *O*,*N*,*S*-thiosemicarbazonate ligands depends on the substituents and degree of deprotonation of the *R*-salicylaldehyde 4*R*′-thiosemicarbazone ligands, the identity of the counter-ion and the nature and degree of solvation (Powell *et al.*, 2014, 2015, 2020, 2022; Powell, 2016; Yemeli Tido, 2010).

In fact, in solution, the free *R*-salicylaldehyde 4*R*′-thiosemicarbazone ligand (H_2L) exists in two tautomeric forms, *i.e.* the thione and thiol forms, as illustrated in Scheme 1. Moreover, the ligand may also be present in its neutral, anionic or dianionic form. We established that the formation of a particular type of Fe^{III} complex unit, *i.e.* neutral, monocationic or monoanionic, can be achieved by tuning the degree of deprotonation of the ligand through pH variation of the reaction solution during the synthesis (Powell *et al.*, 2014, 2015, 2020, 2022; Powell, 2016; Yemeli Tido, 2010; Floquet *et al.*, 2009).

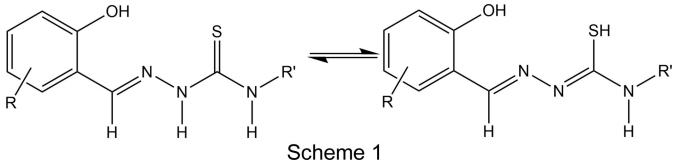

Scheme 1

We have thus been particularly proficient in preparing anionic Fe^{III} complexes of the general formula (cation$^+$)$[Fe(L^{2-})_2]\cdot x$(solvent), such as $Cs[Fe(3\text{-OEt-thsa-Me})_2]\cdot CH_3OH$, containing 3-ethoxysalicylaldehyde methylthiosemicarbazonate(2−) (Powell *et al.*, 2014), $Cs[Fe(5\text{-Br-thsa})_2]$ containing 5-bromosalicylaldehyde thiosemicarbazonate(2−) (Powell *et al.*, 2015) and $NH_4[Fe(thsa)_2]$ containing salicylaldehyde thiosemicarbazonate(2−) (Powell *et al.*, 2020). In all of these compounds, Fe^{III} exhibits the low-spin state.

Here we report a novel Fe^{III} compound of this family, namely, dimethylammonium bis[3-ethoxysalicylaldehyde thiosemicarbazonato(2–)-κ^3O^2,N^1,S]ferrate(III), $[(CH_3)_2NH_2][Fe(3\text{-OEt-thsa})_2]$, (I) (see Scheme 2), containing two dianionic tridentate ligands, *i.e.* 3-ethoxysalicylaldehyde thiosemicarbazonate(2−), whose structure was determined at 100 K and confirmed that Fe^{III} is in the high-spin state.

2. Experimental

2.1. Spectroscopic and magnetic measurements

A room-temperature IR spectrum of 3-ethoxysalicylaldehyde thiosemicarbazone within the range 4000–400 cm^{-1} was recorded on a PerkinElmer FT–IR spectrometer Spectrum RXI using KBr pellets. IR spectroscopic measurements of (I) within the range 4000–600 cm^{-1} were carried out at room temperature using an ATR (attenuated total reflectance) PerkinElmer FT–IR Frontier spectrometer.

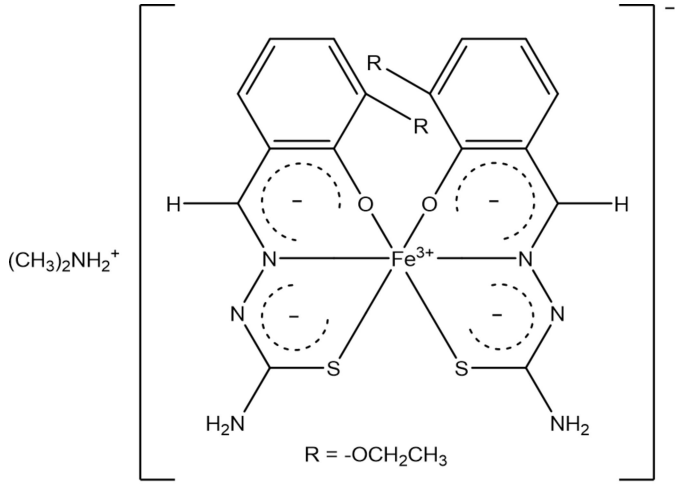

(I)

Scheme 2

^1H and ^{13}C NMR spectra were recorded in DMSO-d_6 (dimethyl sulfoxide) using a Bruker cryomagnet BZH 300/52 spectrometer (300 MHz), with the recorded chemical shifts in δ (in parts per million) relative to an internal standard of tetramethylsilane (TMS).

Measurements of direct current (dc) magnetic susceptibility, χ_M, *versus* temperature, *T*, were conducted between 5 and 320 K, heating and cooling at a rate of 2 K min^{-1} in an applied field, $\mu_0 H$, of 0.1 T using a Quantum Design MPMS-5S superconducting quantum interference device (SQUID) magnetometer. The SQUID magnetometer was calibrated using a standard palladium sample. The background due to the sample holder and the diamagnetic signal of the sample, estimated using Pascal's constants (Bain *et al.*, 2008), was subtracted from the measured molar magnetic susceptibility χ_M.

2.2. Synthesis

The synthesis of 3-ethoxysalicylaldehyde thiosemicarbazone (H_2-3-OEt-thsa) was carried out according to the general procedure described by Yemeli Tido (2010) (yield: 11.14 g, 46.55 mmol, 95.0%; m.p. 224 °C). H_2-3-OEt-thsa is soluble in methanol, ethanol, acetone and DMSO. ^1H NMR (300 MHz, DMSO-d_6): δ (ppm) 11.39 (1H, *s*, OH), 9.02 (1H, *s*, S═C−NH), 8.40 (1H, *s*, N═C−H), 7.90–8.13 (2H, *m*, S═C−NH_2), 6.72–7.50 (aromatic 3H, *m*, C−H), 4.05 (2H, *q*, O−CH_2), 1.35 (3H, *t*, O−C−CH_3). ^{13}C NMR (300 MHz, DMSO-d_6): δ (ppm) 182.8 (C═S), 147.4, 146.7 (C−O), 140.1 (C═N), 119.5, 118.7, 114.5 (C aromatic), 64.6 (C−N), 74.0 (O−CH_2), 15.1 (O−C−CH_3). IR (cm^{-1}, KBr): 3400 (νOH), 3169 (νNH), 3249 (νNH_2), 2935 (νCH_3), 2896 (νCH_2), 1618 (νC═N), 1535–1600 (νC═C), 1270 (νC−N), 1167 (νC═S).

The synthesis of $[(CH_3)_2NH_2][Fe(3\text{-OEt-thsa})_2]$, (I), was carried out as follows: $Fe(NO_3)_3\cdot 9H_2O$ (1.0 mmol, 0.40 g) was

Table 1
Experimental details.

Diffractometer: Rigaku AFC12 goniometer equipped with an enhanced sensitivity (HG) Saturn724+ detector mounted at the window of an FR-E+ SuperBright molybdenum rotating anode generator with VHF Varimax optics (70 µm focus).

Crystal data	
Chemical formula	$(C_2H_8N)[Fe(C_{10}H_{11}N_3O_2S)_2]$
M_r	576.50
Crystal system, space group	Monoclinic, $P2_1/n$
Temperature (K)	100
a, b, c (Å)	9.4359 (3), 16.0265 (5), 17.2333 (7)
β (°)	98.668 (4)
V (Å^3)	2576.35 (17)
Z	4
Radiation type	Mo $K\alpha$
μ (mm^{-1})	0.79
Crystal size (mm)	0.08 × 0.05 × 0.01
Data collection	
Absorption correction	Multi-scan (*CrysAlis PRO*; Agilent, 2014)
T_{min}, T_{max}	0.661, 1.000
No. of measured, independent and observed [$I > 2\sigma(I)$] reflections	16969, 5903, 4415
R_{int}	0.055
(sin $\theta/\lambda)_{max}$ (Å^{-1})	0.649
Refinement	
$R[F^2 > 2\sigma(F^2)]$, $wR(F^2)$, S	0.044, 0.096, 1.02
No. of reflections	5903
No. of parameters	341
No. of restraints	4
H-atom treatment	H atoms treated by a mixture of independent and constrained refinement
$\Delta\rho_{max}$, $\Delta\rho_{min}$ (e Å^{-3})	0.38, −0.38

Computer programs: *CrystalClear-SM Expert* (Rigaku, 2013), *CrysAlis PRO* (Agilent, 2014), *SUPERFLIP* (Palatinus & Chapuis, 2007; Palatinus & van der Lee, 2008), *SHELXL2014* (Sheldrick, 2015), *OLEX2* (Dolomanov *et al.*, 2009) and *ORTEP-3 for Windows* (Farrugia, 2012).

dissolved in water (10 ml). The ligand H_2-3-OEt-thsa (2.0 mmol, 0.46 g) was dissolved in methanol (60 ml) with the addition of dimethylamine, 40 wt% in water (10 mmol, 0.51 ml). To this mixture, the Fe^{III} salt solution was added dropwise with constant stirring. The resulting dark-green solution was stirred and heated to 80 °C for approximately 10 min. The solution was then allowed to stand at room temperature until crystals had formed. The dark-green microcrystals were isolated by filtration and dried (yield: 0.30 g, 0.52 mmol, 52.0%). IR (cm^{-1}, ATR): 3436, 3414 (νNH), 3265, 3098 (νNH$_2$), 3012 (νCH$_3$), 2971 (νCH$_2$), 1614, 1586 (νC═N), 1570–1541 (νC═C ring), 1238 (νC—O), 1215 (νN—N), 1078 (νC—N), 736 (νC—S).

2.3. Refinement

Crystal data, data collection and structure refinement details are summarized in Table 1. The H atoms of terminal amine atoms N103 and N3 were located in difference Fourier maps and refined with restrained N—H distances of 0.86 (2) Å and with U_{iso}(H) = 1.2U_{eq}(N). The remaining H atoms were included in the refinement in calculated positions and treated as riding on their parent atoms, with N—H distances of 0.91 Å and U_{iso}(H) = 1.2U_{eq}(N) for the amine N atom of the cation, C—H distances of 0.95 Å and U_{iso}(H) = 1.2U_{eq}(C) for aryl (–CH═) H atoms, C—H distances of 0.99 Å and U_{iso}(H) = 1.2U_{eq}(C) for secondary (–CH$_2$–) H atoms, and C—H distances of 0.98 Å and U_{iso}(H) = 1.5U_{eq}(C) for methyl (–CH$_3$) H atoms.

Table 2
Selected geometric parameters (Å, °).

Fe1—S1	2.4320 (6)	Fe1—O101	1.9595 (16)
Fe1—S101	2.4389 (7)	Fe1—N1	2.167 (2)
Fe1—O1	1.9806 (16)	Fe1—N101	2.131 (2)
S1—Fe1—S101	98.98 (2)	C108—S101—Fe1	95.71 (8)
O1—Fe1—S1	158.48 (5)	C2—O1—Fe1	127.41 (14)
O1—Fe1—S101	91.30 (5)	C102—O101—Fe1	130.25 (16)
O1—Fe1—N1	82.17 (7)	C7—N1—Fe1	124.80 (15)
O1—Fe1—N101	107.31 (7)	C8—N2—N1	113.96 (19)
O101—Fe1—S1	94.31 (5)	C107—N101—Fe1	123.56 (16)
O101—Fe1—S101	158.89 (5)	C108—N102—N101	114.09 (19)
O101—Fe1—O1	81.91 (7)	C2—C1—C7	121.2 (2)
O101—Fe1—N1	105.56 (7)	O1—C2—C1	122.4 (2)
O101—Fe1—N101	84.03 (7)	N1—C7—C1	125.3 (2)
N1—Fe1—S1	78.45 (5)	N2—C8—S1	125.75 (17)
N1—Fe1—S101	93.18 (5)	C102—C101—C107	121.2 (2)
N101—Fe1—S1	93.26 (5)	O101—C102—C101	123.1 (2)
N101—Fe1—S101	78.93 (5)	N101—C107—C101	125.9 (2)
N101—Fe1—N1	167.63 (7)	N102—C108—S101	125.65 (18)
C8—S1—Fe1	95.87 (8)		

3. Results and discussion

In solution, the free ligand, *i.e.* 3-ethoxysalicylaldehyde thiosemicarbazone (H_2L), exists in two tautomeric forms, the thione and the thiol form, as illustrated in Scheme 1. Consequently, in Fe^{III} compounds, the ligand may be present as either one of the possible tautomers, and may be neutral, anionic or dianionic. Referring to the thiol tautomer, neutral H_2L has H atoms located on the phenol O atom and the thiol S atom. The first deprotonation step involving the phenol group results in the formation of 3-ethoxysalicylaldehyde thiosemicarbazone(1−) (abbreviated as HL^-). Subsequent deprotonation yields 3-ethoxysalicylaldehyde thiosemicarbazonate(2−) (abbreviated as L^{2-}).

The structure of dimethylammonium bis[3-ethoxysalicylaldehyde thiosemicarbazonato(2−)-κ^3O^2,N^1,S]ferrate(III), (I) (Fig. 1), was determined at 100 K. Compound (I) crystallized in the monoclinic space group $P2_1/n$, with Z = 4. The asymmetric unit consists of one formula unit, $[(CH_3)_2NH_2][Fe(3\text{-}OEt\text{-}thsa)_2]$, with no atom on a special position. The Fe^{III} cation is coordinated by the thiolate S, phenolate O and imine N atoms of each of the two dianionic *O*,*N*,*S*-tridentate L^{2-} ligands. The donor atoms of the ligands are situated in two perpendicular planes, with the O and S atoms in *cis* positions, and mutually *trans* N atoms. Selected geometric parameters are listed in Table 2.

The $Fe^{III}O_2N_2S_2$ coordination sphere exhibits a distorted octahedral geometry, as evidenced by the bond angles of the Fe atom and the ligand donor atoms (*vide infra*). X-ray structural data of similar Fe^{III}–bis(ligand) compounds containing two dianionic thiosemicarbazonate(2−) ligands show

that the Fe—S, Fe—O and Fe—N bond lengths are in the ranges 2.23–2.31, 1.93–1.95 and 1.88–1.96 Å, respectively, for low-spin Fe^{III} compounds, and in the ranges 2.40–2.44, 1.96–1.99 and 2.05–2.15 Å, respectively, for the corresponding high-spin Fe^{III} compounds (van Koningsbruggen *et al.*, 2004). The bond lengths involving the Fe atom and the donor atoms in (I) correspond with Fe^{III} being in the high-spin state at 100 K.

Variable-temperature magnetic susceptibility measurements (5–320 K) confirm that the Fe^{III} ion in (I) is indeed in the high-spin state over this temperature range (Powell, 2016). High-spin Fe^{III} has also been evidenced in the related $Cs[Fe(thsa)_2]$ compound at 103 (and 298 K) (Ryabova *et al.*, 1981*a*). It is significant to note that the Fe—O distances seem to be less sensitive to the change in Fe^{III} spin state than the Fe—N and Fe—S distances, which may be related to the π-acceptor capability of the N- and S-donor atoms as opposed to the π-donor capability of the O-donor atoms. This is of particular significance when Fe^{III} is in the low-spin state, as increased π backbonding will lead to comparatively more pronounced shortening of the Fe—N and Fe—S bonds than of the Fe—O bonds (Powell *et al.*, 2014).

Furthermore, the spin state of the Fe^{III} cation can be related to the bond angles of the $FeO_2N_2S_2$ coordination core. An analysis of the bond angles involving the opposite ligand donor atoms at 100 K is very enlightening, as it shows that the octahedral geometry of the present high-spin Fe^{III} compound, with O1—Fe1—S1 = 158.48 (5)°, O101—Fe1—S101 = 158.89 (5)° and N1—Fe1—N101 = 167.63 (7)°, is considerably less regular than that of the low-spin compound $Cs[Fe(3\text{-OEt-thsa-Me})_2]\cdot CH_3OH$, with the bond angles S11—Fe—O11 = 177.83 (14)°, S21—Fe—O21 = 178.01 (13)° and N11—Fe—N21 = 178.9 (2)° (Powell *et al.*, 2014), which are closer to 180°. This is in agreement with the low-spin Fe^{III} ion adopting a more regular octahedral geometry than the high-spin Fe^{III} ion (van Koningsbruggen *et al.*, 2004).

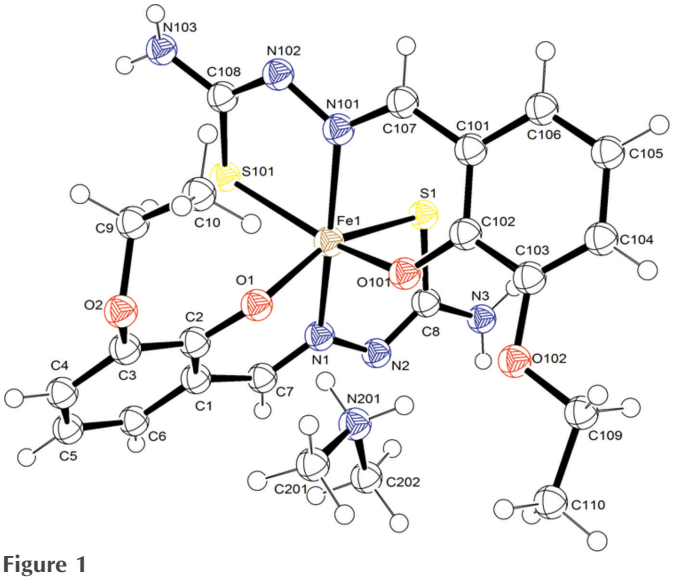

Figure 1
The molecular structure and atom-numbering scheme for (I). Displacement ellipsoids are drawn at the 50% probability level.

The ligands have been found to be in the dianionic form as no H atoms were located on the phenolate O (O1 and O101) or the thiolate S (S1 and S101) atoms. The charge of the two L^{2-} ligands is balanced by the presence of the monovalent dimethylammonium cation together with the trivalent iron cation. The tridentate ligands of the present compound are coordinated to the Fe^{III} cation by the thiolate S, phenolate O and imine N atoms, forming six- and five-membered chelate rings. The six-membered chelate ring involves a significantly less restricted bite angle [O1—Fe—N1 = 82.17 (7)° and O101—Fe—N101 = 84.03 (7)°] than the five-membered chelate ring [S1—Fe—N1 = 78.45 (5)° and S101—Fe—N101 = 78.93 (5)°]. The r.m.s. deviations from their least-squares plane of atoms of the six-membered chelate ring of both coordinated ligands are 0.197 and 0.177 Å for Fe1/N11/C17/C11/C12/O11 and Fe1/N101/C107/C101/C102/O101, respectively, and the corresponding values for the five-membered chelate rings are 0.129 and 0.102 Å for Fe1/N11/C12/C18/S11 and Fe1/N101/C102/C108/S101, respectively. It appears that the metal chelate rings deviate slightly from the ideal planar structure. Furthermore, the O—Fe—N and S—Fe—N bite angles of the six- and five-membered chelates are deficient by *ca* 38 and 30°, respectively, compared to the angle at the vertex of a regular hexagon (120°) or pentagon (108°), respectively. In comparison to other $(cation^{+})[Fe(L^{2-})_2]\cdot x$(solvent) compounds of related ligands (Powell *et al.*, 2014, 2015, 2020), the deficiency of the bite angle in both the six- and five-membered chelate rings is larger than expected, though it has been recognized that these other Fe^{III} bis(ligand) compounds contain Fe^{III} in the low-spin state, whereas the present compound contains Fe^{III} in the high-spin state. Consequently, (I) displays longer Fe^{III}–donor atom bond lengths, which are associated with more restricted bite angles. Moreover, the remaining bond angles involving each six-membered chelate ring (Table 2) are, as expected, within *ca* 5° of the value of 125°. However, the C—S—Fe bond angles involving each five-membered chelate ring are only about 95°, providing an additional deficiency of 13°. The additional deficiency can be offset by increasing the other bond angles within this five-membered chelate ring to *ca* 120°. It has been found that the N—N—C angles are <120° and the N—C—S angles are >120°; these values suggest sp^2 hybridization at the C and N atoms.

The stability of the Fe^{III} complex is further enhanced by the high degree of electron delocalization throughout the chelated ligands, which is evident from the geometric parameters. The C—S, C—N and N—N bond lengths of (I) show characteristics of a bond order between 1 (*i.e.* single bond) and 2 (*i.e.* double bond). The C8—S1 bond length of 1.746 (3) Å and the C108—S101 bond length of 1.752 (2) Å suggest partial electron delocalization of these C—S bonds. This feature has also been found in the structure of the related high-spin Fe^{III} compound $Cs[Fe(thsa)_2]$ at 103 K (Ryabova *et al.*, 1981*a*), in which the C—S bond lengths of 1.749 (9) and 1.761 (9) Å are indicative of partial electron delocalization.

In addition, the electron delocalization within each of the *O*,*N*,*S*-tridentate ligands is confirmed by a bond order larger than 1 for the C—N bond involving the deprotonated hydra-

zinic N atom, which is inferred from the lengths for the C7—N1 and C107—N101 bonds in (I) at 100 K of 1.301 (3) and 1.301 (3) Å, respectively, which correspond to the C—N bond lengths of 1.314 (10) and 1.303 (11) Å, respectively, for Cs[Fe(thsa)$_2$] at 103 K (Ryabova *et al.*, 1981*a*).

Moreover, the N—N bond lengths of (I) at 100 K are N1—N2 of 1.395 (2) Å and N101—N102 of 1.399 (3) Å, which indicates partial electron delocalization within the five-membered chelate ring.

The hydrogen-bonding interactions of (I), identified using the default parameters of *OLEX2* (Dolomanov *et al.*, 2009), are listed in Table 3 and displayed in Fig. 2. The N atom of the dimethylammonium cation forms two hydrogen bonds: one contact is formed with the phenolate O atom of one ligand, whereas the second contact is formed with the ethoxy O atom of the salicylaldehyde moiety of the other ligand. The N201—H20*A*···O102 and N201—H20*B*···O1 contacts form an intramolecular hydrogen-bonded ring system, giving rise to an $R_2^2(9)$ ring (Bernstein *et al.*, 1995).

Magnetic susceptibility *versus* temperature measurements for (I) were carried out to investigate the spin state of the Fe^{III} ion. The data collected on heating and cooling coincide over the temperature range studied. The temperature dependence of $\chi_M T$ collected on cooling between 320 and 5 K is displayed in Fig. 3. Above 100 K, $\chi_M T$ is temperature independent with a value of 4.41 (1) cm^3 K mol^{-1} [5.94 (1) μ_B/Fe]. This is just above the expected value of 4.38 cm^3 K mol^{-1} (5.92 μ_B/Fe) for Fe^{III} in its high-spin (S = 5/2) state with an electronic g factor of 2. $\chi_M^{-1}(T)$ is linear in T and a fit to a Curie–Weiss law between 100 and 320 K shown in Fig. 4 gives a Weiss temperature of −3.3 (1) K and an effective moment of 6.00 (1) μ_B/Fe.

$\chi_M T$ drops rapidly below 100 K. This may be due to weak (antiferro)magnetic interactions between neighbouring spins or may reflect a splitting of the S = 5/2 state (O'Connor, 1982). Studies using aligned single crystals are needed to differentiate between these possibilities. For splitting, the spin Hamiltonian can be written as $H_S = H_{CEF} + H_z$, where the crystalline electric field (CEF) term $H_{CEF} = D[S_z^2 - S(S+1)/3] + E(S_x^2 - S_y^2)$, with D and E being the axial and rhombic zero-field splitting, respectively. The ^6S high-spin state is split into three Kramers doublets. For E = 0, the doublets are separated by 2D and 6D from the lowest energy doublet. The Zeeman energy $H_z = g\mu_B H S_z$ and the molar susceptibility with a field along z is

$$\chi_M = \frac{N_A g^2 \mu_B^2}{4k_B T}\left[\frac{1 + 9e^{-2X} + 25e^{-6X}}{1 + e^{-2X} + e^{-6X}}\right], \qquad (1)$$

where $X = D/k_B T$, N_A is Avogadro's number and k_B is the Boltzmann constant (O'Connor, 1982). A fit gives D = 0.83 (1) cm^{-1} with g = 2. D is in the range expected for high-spin Fe^{III} (Chen *et al.*, 2002; Yemeli Tido *et al.*, 2007). Fits with a finite E expected for a system with a rhombic distortion are possible, *cf.* Chen *et al.* (2002), but these require a knowledge of the ratio $\lambda = E/D$ from other studies, such as electron paramagnetic resonance (EPR) spectroscopy.

It is of interest to compare the two Fe^{III} compounds that have so far been reported to contain the 3-ethoxysalicylaldehyde 4-R'-thiosemicarbazonate(2−) dianion. In Cs[Fe(3-OEt-thsa-Me)$_2$]·CH$_3$OH (Powell *et al.*, 2014), Fe^{III} is low spin, whereas in the present [(CH$_3$)$_2$NH$_2$][Fe(3-OEt-thsa)$_2$] compound, (I), the metal ion adopts the high-spin state. The differences between the two compounds further involve: (i) the relative size of the R' substituent on the terminal N atom of the thiosemicarbazide moiety, as (I) contains a H atom, whereas Cs[Fe(3-OEt-thsa-Me)$_2$]·CH$_3$OH (Powell *et al.*, 2014) contains a methyl substituent; (ii) the difference in the size and intermolecular interactions involving the associated outer-sphere monovalent cation, *i.e.* (CH$_3$)$_2$NH$_2^+$ *versus* Cs$^+$; and

Table 3
Hydrogen-bond geometry (Å, °).

D—H···A	D—H	H···A	D···A	D—H···A
N201—H20*A*···O102	0.91	1.97	2.877 (3)	174
N201—H20*B*···O1	0.91	1.86	2.766 (3)	173

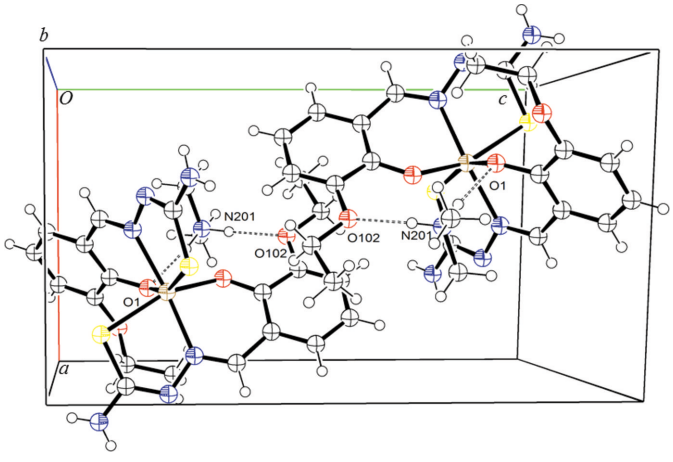

Figure 2
The unit cell of (I), with displacement ellipsoids drawn at the 50% probability level.

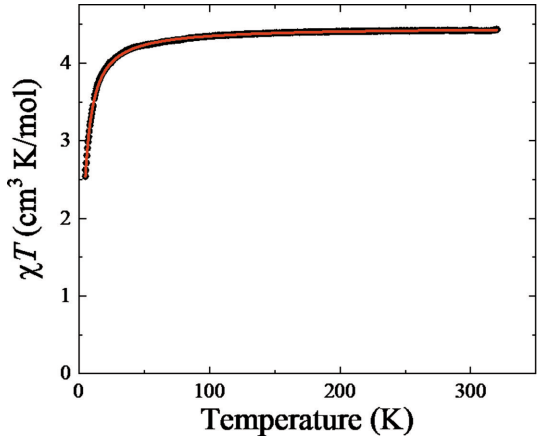

Figure 3
$\chi_M T$ *versus* T for (I). The data were measured while cooling at a rate of 2 K min^{-1} in an applied field $\mu_0 H$ of 0.1 T.

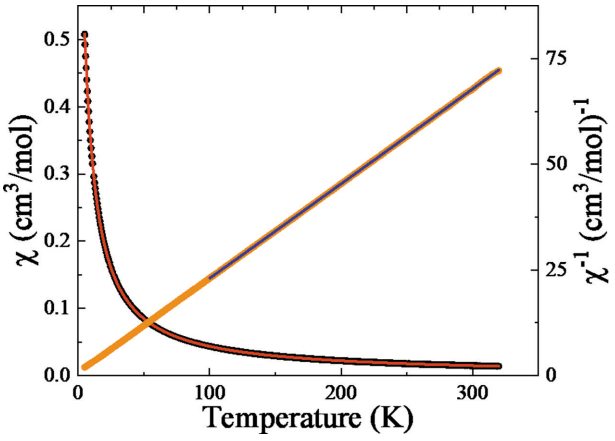

Figure 4
Temperature dependence of the molar magnetic susceptibility, χ_M, for (I). The solid red lines show fits to the data using Equation (1), with D = 0.83 (1) cm^{-1} and g = 2. The blue line shows a fit of $\chi_M{}^{-1}(T)$ above 100 K using a Curie–Weiss law.

(iii) the presence of a methanol solvent molecule in the crystal lattice of Cs[Fe(3-OEt-thsa-Me)$_2$]·CH$_3$OH (Powell *et al.*, 2014). These differences are associated with (I) forming intramolecular ring systems through hydrogen bonds (*vide supra*), whereas Cs[Fe(3-OEt-thsa-Me)$_2$]·CH$_3$OH forms intermolecular hydrogen-bonded ring systems which link neighbouring Fe^{III} entities. These factors determine the arrangement of the Fe^{III} entities within the unit cell, which is further characterized by the space group $P2_1/n$, with Z = 4 and V = 2576.35 (17) Å^3 for (I), with a volume of 644.09 Å^3 per high-spin Fe^{III} formula unit, and the space group $P\overline{1}$, with Z = 2 and V = 1369.5 (8) Å^3 for Cs[Fe(3-OEt-thsa-Me)$_2$]·CH$_3$OH, with a volume of 684.75 Å^3 per low-spin Fe^{III} formula unit (Powell *et al.*, 2014); hence the volume increase associated with Fe^{III} being low-spin compared to high-spin is more than offset by the differences in substituents, composition and crystal packing.

Evidently, the intricate interplay between the variation in cation, ligand substituents and associated solvent molecules affects the crystal packing of compounds of this class of (cation$^+$)[Fe(L^{2-})$_2$]·x(solvent) materials and allows for a variation of the spin state of Fe^{III}, with some members displaying temperature-dependent spin-crossover behaviour (van Koningsbruggen *et al.*, 2004; Powell, 2016). Further studies by our group will additionally focus on tuning the spin state of Fe^{III} by varying the degree of deprotonation of the ligand.

Acknowledgements

We thank the EPSRC UK National Crystallography Service (Coles & Gale, 2012) at the University of Southampton for the collection of the crystallographic data.

References

Agilent (2014). *CrysAlis PRO*. Agilent Technologies Ltd, Yarnton, Oxfordshire, England.
Bain, G. A. & Berry, J. F. (2008). *J. Chem. Educ.* **85**, 532–536.
Bernstein, J., Davis, R. E., Shimoni, L. & Chang, N.-L. (1995). *Angew. Chem. Int. Ed. Engl.* **34**, 1555–1573.
Cambi, L. & Szegö, L. (1931). *Berichte*, **64**, 2591–2598.
Cambi, L. & Szegö, L. (1933). *Berichte*, **66**, 656–661.
Chen, C.-H., Lee, Y.-Y., Liau, B.-C., Elango, S., Chen, J.-H., Hsieh, H.-Y., Liao, F.-L., Wang, S.-L. & Hwang, L.-P. (2002). *J. Chem. Soc. Dalton Trans.* pp. 3001–3006.
Coles, S. J. & Gale, P. A. (2012). *Chem. Sci.* **3**, 683–689.
Dolomanov, O. V., Bourhis, L. J., Gildea, R. J., Howard, J. A. K. & Puschmann, H. (2009). *J. Appl. Cryst.* **42**, 339–341.
Farrugia, L. J. (2012). *J. Appl. Cryst.* **45**, 849–854.
Floquet, S., Boillot, M. L., Rivière, E., Varret, F., Boukheddaden, K., Morineau, D. & Négrier, P. (2003). *New J. Chem.* **27**, 341–348.
Floquet, S., Guillou, N., Négrier, P., Rivière, E. & Boillot, M. L. (2006). *New J. Chem.* **30**, 1621–1627.
Floquet, S., Muñoz, M. C., Guillot, R., Rivière, E., Blain, G., Réal, J. A. & Boillot, M. L. (2009). *Inorg. Chim. Acta*, **362**, 56–64.
Gütlich, P. & Goodwin, H. A. (2004). *Top. Curr. Chem.* **233**, 1–47.
Gütlich, P., van Koningsbruggen, P. J. & Renz, F. (2004). *Struct. Bond.* **107**, 27–75.
Halcrow, M. A. (2013). Editor. In *Spin-Crossover Materials*. Oxford: John Wiley & Sons Ltd.
Harding, D. J., Harding, P. & Phonsri, W. (2016). *Coord. Chem. Rev.* **313**, 38–61.
Hayami, S., Gu, Z., Shiro, M., Einaga, Y., Fujishima, A. & Sato, O. (2000). *J. Am. Chem. Soc.* **122**, 7126–7127.
Hayami, S., Hiki, K., Kawahara, T., Maeda, Y., Urakami, D., Inoue, K., Ohama, M., Kawata, S. & Sato, O. (2009). *Chem. Eur. J.* **15**, 3497–3508.
Karuppannan, S. K., Martín-Rodríguez, A., Ruiz, E., Harding, P., Harding, D. J., Yu, X., Tadich, A., Cowie, B., Qi, D. & Nijhuis, C. A. (2021). *Chem. Sci.* **12**, 2381–2388.
Koningsbruggen, P. J. van, Maeda, Y. & Oshio, H. (2004). *Top. Curr. Chem.* **233**, 259–324.
Létard, J. F., Guionneau, P. & Goux-Capes, L. (2004). *Top. Curr. Chem.* **235**, 221–249.
Li, Z. Y., Dai, J. W., Shiota, Y., Yoshizawa, K., Kanegawa, S. & Sato, O. (2013). *Chem. Eur. J.* **19**, 12948–12952.
Li, Z.-Y., Ohtsu, H., Kojima, T., Dai, J.-W., Yoshida, T., Breedlove, B. K., Zhang, W.-X., Iguchi, H., Sato, O., Kawano, M. & Yamashita, M. (2016). *Angew. Chem. Int. Ed.* **55**, 5184–5189.
Molnár, G., Rat, S., Salmon, L., Nicolazzi, W. & Bousseksou, A. (2018). *Adv. Mater.* **30**, 1703862.
O'Connor, C. J. (1982). *Progress in Inorganic Chemistry*, edited by S. J. Lippard, Vol. 29, pp. 203–283. New York: John Wiley & Sons, Inc.
Palatinus, L. & Chapuis, G. (2007). *J. Appl. Cryst.* **40**, 786–790.
Palatinus, L. & van der Lee, A. (2008). *J. Appl. Cryst.* **41**, 975–984.
Phonsri, W., Darveniza, L. C., Batten, S. R. & Murray, K. S. (2017). *Inorganics*, **5**, 51.
Powell, R. E. (2016). PhD thesis, Aston University, Birmingham, UK.
Powell, R. E., Lees, M. R., Tizzard, G. J. & van Koningsbruggen, P. J. (2022). *Acta Cryst.* C**78**, 63–69.
Powell, R. E., Schwalbe, C. H., Tizzard, G. J. & van Koningsbruggen, P. J. (2014). *Acta Cryst.* C**70**, 595–598.
Powell, R. E., Schwalbe, C. H., Tizzard, G. J. & van Koningsbruggen, P. J. (2015). *Acta Cryst.* C**71**, 169–174.
Powell, R. E., Stöger, B., Knoll, C., Müller, D., Weinberger, P. & van Koningsbruggen, P. J. (2020). *Acta Cryst.* C**76**, 625–631.
Rigaku (2013). *CrystalClear-SM Expert*. Riguku Corporation, The Woodlands, Texas, USA.
Rubio-Giménez, V., Bartual-Murgui, C., Galbiati, M., Núñez-López, A., Castells-Gil, J., Quinard, B., Seneor, P., Otero, E., Ohresser, P., Cantarero, A., Coronado, E., Real, J. A., Mattana, R., Tatay, S. & Martí-Gastaldo, C. (2019). *Chem. Sci.* **10**, 4038–4047.
Ryabova, N. A., Ponomarev, V. I., Atovmyan, L. O., Zelentsov, V. V. & Shipilov, V. I. (1978). *Koord. Khim.* **4**, 119.

Ryabova, N. A., Ponomarev, V. I., Zelentsov, V. V. & Atovmyan, L. O. (1981*a*). *Kristallografiya*, **26**, 101–108.
Ryabova, N. A., Ponomarev, V. I., Zelentsov, V. V. & Atovmyan, L. O. (1982). *Kristallografiya*, **27**, 81–91.
Ryabova, N. A., Ponomarev, V. I., Zelentsov, V. V., Shipilov, V. I. & Atovmyan, L. O. (1981*b*). *J. Struct. Chem.* **22**, 234–238.
Senthil Kumar, K. & Ruben, M. (2017). *Coord. Chem. Rev.* **346**, 176–205.
Sheldrick, G. M. (2015). *Acta Cryst.* C**71**, 3–8.
Tissot, A., Kesse, X., Giannopoulou, S., Stenger, I., Binet, L., Rivière, E. & Serre, C. (2019). *Chem. Commun.* **55**, 194–197.
Yemeli Tido, E. W. (2010). PhD thesis, University of Groningen, The Netherlands.
Yemeli Tido, E. W., Vertelman, E. J. M., Meetsma, A. & van Koningsbruggen, P. J. (2007). *Inorg. Chim. Acta*, **360**, 3896–3902.
Zelentsov, V. V., Bogdanova, L. G., Ablov, A. V., Gerbeleu, N. V. & Dyatlova, C. V. (1973). *Russ. J. Inorg. Chem.* **18**, 2654-2657.

supporting information

Acta Cryst. (2023). C**79** [https://doi.org/10.1107/S2053229622011597]

Fe^{III} in the high-spin state in dimethylammonium bis[3-ethoxysalicylaldehyde thiosemicarbazonato(2–)-κ^3O^2,N^1,S]ferrate(III)

Robyn E. Powell, Martin R. Lees, Graham J. Tizzard, Simon J. Coles, Qingchun Yuan and Petra J. van Koningsbruggen

Computing details

Data collection: *CrystalClear*-SM Expert (Rigaku, 2013); cell refinement: *CrysAlis PRO* (Agilent, 2014); data reduction: *CrysAlis PRO* (Agilent, 2014); program(s) used to solve structure: Superflip (Palatinus & Chapuis, 2007; Palatinus & van der Lee, 2008; Palatinus *et al.*, 2012); program(s) used to refine structure: *SHELXL2014* (Sheldrick, 2015); molecular graphics: OLEX2 (Dolomanov *et al.*, 2009); software used to prepare material for publication: OLEX2 (Dolomanov *et al.*, 2009).

Dimethylammonium bis[3-ethoxysalicylaldehyde thiosemicarbazonato(2-)-κ^3O^2,N^1,S]ferrate(III)

Crystal data

$(C_2H_8N)[Fe(C_{10}H_{11}N_3O_2S)_2]$
$M_r = 576.50$
Monoclinic, $P2_1/n$
$a = 9.4359$ (3) Å
$b = 16.0265$ (5) Å
$c = 17.2333$ (7) Å
$\beta = 98.668$ (4)°
$V = 2576.35$ (17) Å^3
$Z = 4$
$F(000) = 1204$
$D_x = 1.486$ Mg m^{-3}
Mo $K\alpha$ radiation, $\lambda = 0.71075$ Å
Cell parameters from 7929 reflections
$\theta = 2.3$–27.5°
$\mu = 0.79$ mm^{-1}
$T = 100$ K
Plate, dark green
0.08 × 0.05 × 0.01 mm

Data collection

Rigaku AFC12 (Right) diffractometer
Radiation source: Rotating Anode, Rigaku FRE+
Confocal mirrors, VHF Varimax monochromator
Detector resolution: 28.5714 pixels mm^{-1}
profile data from ω–scans
Absorption correction: multi-scan (CrysAlis PRO; Agilent, 2014)
$T_{min} = 0.661$, $T_{max} = 1.000$
16969 measured reflections
5903 independent reflections
4415 reflections with $I > 2\sigma(I)$
$R_{int} = 0.055$
$\theta_{max} = 27.5°$, $\theta_{min} = 2.3°$
$h = -12\rightarrow11$
$k = -19\rightarrow20$
$l = -22\rightarrow20$

Refinement

Refinement on F^2
Least-squares matrix: full
$R[F^2 > 2\sigma(F^2)] = 0.044$
$wR(F^2) = 0.096$
$S = 1.02$
5903 reflections
341 parameters
4 restraints
Primary atom site location: iterative
Hydrogen site location: mixed

H atoms treated by a mixture of independent and constrained refinement
$w = 1/[\sigma^2(F_o^2) + (0.042P)^2 + 0.8071P]$ where $P = (F_o^2 + 2F_c^2)/3$

$(\Delta/\sigma)_{max} = 0.001$
$\Delta\rho_{max} = 0.38$ e Å^{-3}
$\Delta\rho_{min} = -0.37$ e Å^{-3}

Special details

Geometry. All esds (except the esd in the dihedral angle between two l.s. planes) are estimated using the full covariance matrix. The cell esds are taken into account individually in the estimation of esds in distances, angles and torsion angles; correlations between esds in cell parameters are only used when they are defined by crystal symmetry. An approximate (isotropic) treatment of cell esds is used for estimating esds involving l.s. planes.

Refinement. H atoms bonded to N3 and N103 were located in the difference map and then refined with U_{iso} 1.2 times the parent atoms and a geometrical distance restraint

Fractional atomic coordinates and isotropic or equivalent isotropic displacement parameters (Å^2)

	x	*y*	*z*	U_{iso}*/U_{eq}
Fe1	0.70898 (4)	0.21635 (2)	0.50186 (2)	0.00856 (10)
S1	0.62044 (6)	0.25318 (4)	0.62279 (3)	0.01270 (14)
S101	0.84413 (7)	0.09133 (4)	0.54708 (4)	0.01227 (14)
O1	0.70288 (17)	0.18269 (10)	0.39082 (9)	0.0110 (4)
O2	0.84874 (18)	0.12675 (10)	0.27538 (10)	0.0161 (4)
O101	0.66835 (17)	0.32616 (10)	0.45361 (9)	0.0119 (4)
O102	0.52885 (18)	0.45436 (10)	0.38418 (9)	0.0137 (4)
N1	0.5051 (2)	0.15161 (12)	0.48756 (11)	0.0106 (4)
N2	0.3979 (2)	0.17493 (12)	0.53078 (12)	0.0117 (4)
N3	0.3409 (2)	0.25363 (14)	0.63117 (13)	0.0153 (5)
H3A	0.256 (2)	0.2433 (17)	0.6111 (15)	0.018*
H3B	0.369 (3)	0.2879 (14)	0.6684 (13)	0.018*
N101	0.9159 (2)	0.26779 (12)	0.54029 (11)	0.0103 (4)
N102	1.0392 (2)	0.21832 (12)	0.55538 (11)	0.0104 (4)
N103	1.1288 (2)	0.08691 (13)	0.56251 (13)	0.0157 (5)
H10A	1.116 (3)	0.0359 (11)	0.5552 (15)	0.019*
H10B	1.209 (2)	0.1093 (16)	0.5565 (16)	0.019*
C1	0.5548 (2)	0.05970 (14)	0.38160 (14)	0.0107 (5)
C2	0.6673 (3)	0.10847 (15)	0.35927 (13)	0.0104 (5)
C3	0.7393 (3)	0.07927 (15)	0.29831 (14)	0.0140 (5)
C4	0.6979 (3)	0.00603 (15)	0.25903 (14)	0.0154 (6)
H4	0.7461	−0.0122	0.2175	0.019*
C5	0.5848 (3)	−0.04148 (16)	0.28023 (14)	0.0173 (6)
H5	0.5567	−0.0919	0.2532	0.021*
C6	0.5141 (3)	−0.01476 (15)	0.34072 (14)	0.0144 (5)
H6	0.4374	−0.0470	0.3547	0.017*
C7	0.4709 (3)	0.08925 (15)	0.44005 (14)	0.0117 (5)
H7	0.3840	0.0608	0.4439	0.014*
C8	0.4427 (3)	0.22466 (14)	0.59064 (14)	0.0118 (5)
C9	0.9693 (3)	0.14200 (17)	0.33761 (15)	0.0200 (6)
H9A	1.0543	0.1106	0.3264	0.024*
H9B	0.9449	0.1221	0.3884	0.024*
C10	1.0037 (3)	0.23397 (18)	0.34309 (17)	0.0275 (7)

H10C	1.0318	0.2530	0.2935	0.041*
H10D	1.0828	0.2436	0.3860	0.041*
H10E	0.9190	0.2650	0.3533	0.041*
C101	0.8381 (3)	0.41371 (14)	0.53308 (14)	0.0107 (5)
C102	0.7139 (3)	0.40090 (14)	0.47803 (14)	0.0099 (5)
C103	0.6384 (3)	0.47241 (15)	0.44448 (14)	0.0116 (5)
C104	0.6755 (3)	0.55135 (15)	0.47206 (14)	0.0150 (5)
H104	0.6206	0.5981	0.4513	0.018*
C105	0.7940 (3)	0.56275 (15)	0.53065 (15)	0.0156 (6)
H105	0.8172	0.6170	0.5509	0.019*
C106	0.8772 (3)	0.49560 (15)	0.55903 (15)	0.0143 (5)
H106	0.9611	0.5042	0.5962	0.017*
C107	0.9385 (3)	0.34655 (14)	0.55569 (14)	0.0110 (5)
H107	1.0290	0.3613	0.5844	0.013*
C108	1.0136 (3)	0.13784 (15)	0.55374 (13)	0.0115 (5)
C109	0.4454 (3)	0.52495 (15)	0.34938 (14)	0.0150 (5)
H10F	0.5089	0.5660	0.3290	0.018*
H10G	0.3965	0.5528	0.3893	0.018*
C110	0.3359 (3)	0.49200 (16)	0.28312 (16)	0.0218 (6)
H11A	0.3854	0.4694	0.2416	0.033*
H11B	0.2722	0.5375	0.2618	0.033*
H11C	0.2794	0.4478	0.3031	0.033*
N201	0.5046 (2)	0.29205 (13)	0.31206 (12)	0.0164 (5)
H20A	0.5147	0.3449	0.3314	0.020*
H20B	0.5729	0.2598	0.3406	0.020*
C201	0.5291 (3)	0.29274 (18)	0.22933 (16)	0.0258 (7)
H20C	0.4541	0.3258	0.1978	0.039*
H20D	0.5265	0.2354	0.2093	0.039*
H20E	0.6230	0.3175	0.2260	0.039*
C202	0.3612 (3)	0.26016 (19)	0.32239 (17)	0.0282 (7)
H20F	0.2870	0.2954	0.2929	0.042*
H20G	0.3515	0.2613	0.3782	0.042*
H20H	0.3503	0.2027	0.3029	0.042*

Atomic displacement parameters (Å²)

	U^{11}	U^{22}	U^{33}	U^{12}	U^{13}	U^{23}
Fe1	0.00729 (18)	0.00775 (18)	0.01073 (18)	−0.00032 (14)	0.00164 (13)	−0.00020 (13)
S1	0.0093 (3)	0.0159 (3)	0.0132 (3)	−0.0012 (3)	0.0025 (2)	−0.0035 (2)
S101	0.0096 (3)	0.0095 (3)	0.0177 (3)	−0.0001 (2)	0.0021 (2)	0.0006 (2)
O1	0.0119 (9)	0.0094 (9)	0.0121 (9)	−0.0015 (7)	0.0028 (7)	−0.0021 (7)
O2	0.0157 (10)	0.0200 (10)	0.0136 (9)	−0.0029 (8)	0.0049 (7)	−0.0004 (7)
O101	0.0135 (9)	0.0076 (9)	0.0140 (9)	0.0003 (7)	0.0003 (7)	−0.0006 (7)
O102	0.0166 (10)	0.0093 (9)	0.0145 (9)	0.0046 (7)	−0.0003 (7)	0.0016 (7)
N1	0.0104 (11)	0.0108 (10)	0.0109 (10)	0.0010 (8)	0.0023 (8)	0.0009 (8)
N2	0.0087 (11)	0.0130 (11)	0.0144 (11)	−0.0008 (8)	0.0051 (8)	−0.0024 (8)
N3	0.0097 (11)	0.0175 (12)	0.0194 (12)	−0.0023 (10)	0.0047 (9)	−0.0064 (9)
N101	0.0069 (10)	0.0132 (11)	0.0109 (10)	0.0005 (8)	0.0018 (8)	0.0005 (8)

N102	0.0058 (10)	0.0107 (10)	0.0143 (11)	0.0019 (8)	−0.0001 (8)	−0.0002 (8)
N103	0.0097 (11)	0.0107 (11)	0.0264 (13)	−0.0001 (10)	0.0020 (9)	−0.0026 (9)
C1	0.0097 (13)	0.0095 (12)	0.0122 (12)	0.0020 (10)	−0.0008 (10)	0.0007 (9)
C2	0.0097 (13)	0.0111 (12)	0.0094 (12)	0.0033 (10)	−0.0020 (9)	−0.0002 (9)
C3	0.0123 (13)	0.0159 (13)	0.0138 (13)	0.0013 (10)	0.0023 (10)	0.0012 (10)
C4	0.0199 (14)	0.0174 (14)	0.0097 (13)	0.0036 (11)	0.0045 (11)	−0.0027 (10)
C5	0.0234 (15)	0.0123 (13)	0.0144 (13)	−0.0012 (11)	−0.0031 (11)	−0.0051 (10)
C6	0.0151 (14)	0.0100 (13)	0.0170 (13)	−0.0013 (10)	−0.0014 (10)	0.0014 (10)
C7	0.0093 (13)	0.0108 (12)	0.0151 (13)	−0.0018 (10)	0.0018 (10)	0.0014 (9)
C8	0.0114 (13)	0.0104 (12)	0.0142 (13)	−0.0004 (10)	0.0041 (10)	0.0031 (9)
C9	0.0148 (14)	0.0293 (16)	0.0159 (14)	−0.0016 (12)	0.0019 (11)	−0.0041 (11)
C10	0.0275 (17)	0.0341 (18)	0.0220 (15)	−0.0162 (14)	0.0071 (13)	−0.0039 (12)
C101	0.0098 (12)	0.0089 (12)	0.0142 (13)	−0.0004 (10)	0.0042 (10)	−0.0001 (9)
C102	0.0128 (13)	0.0079 (12)	0.0104 (12)	0.0005 (10)	0.0061 (10)	0.0011 (9)
C103	0.0103 (13)	0.0117 (12)	0.0137 (13)	0.0014 (10)	0.0047 (10)	0.0013 (9)
C104	0.0186 (14)	0.0106 (13)	0.0173 (13)	0.0032 (11)	0.0073 (11)	0.0037 (10)
C105	0.0174 (14)	0.0094 (13)	0.0212 (14)	−0.0020 (11)	0.0067 (11)	−0.0035 (10)
C106	0.0112 (13)	0.0127 (13)	0.0191 (14)	−0.0030 (10)	0.0023 (10)	−0.0036 (10)
C107	0.0090 (13)	0.0111 (12)	0.0124 (12)	−0.0017 (10)	0.0005 (10)	0.0007 (9)
C108	0.0116 (13)	0.0133 (13)	0.0096 (12)	0.0020 (10)	0.0019 (10)	0.0008 (9)
C109	0.0153 (14)	0.0136 (13)	0.0168 (13)	0.0060 (11)	0.0046 (11)	0.0061 (10)
C110	0.0223 (15)	0.0217 (15)	0.0209 (15)	0.0078 (12)	0.0014 (12)	0.0061 (11)
N201	0.0182 (12)	0.0157 (12)	0.0135 (11)	0.0040 (9)	−0.0035 (9)	0.0002 (9)
C201	0.0339 (18)	0.0268 (16)	0.0171 (15)	0.0033 (13)	0.0047 (13)	−0.0020 (12)
C202	0.0231 (16)	0.0317 (17)	0.0290 (17)	0.0007 (13)	0.0015 (13)	0.0074 (13)

Geometric parameters (Å, º)

Fe1—S1	2.4320 (6)	C6—H6	0.9500
Fe1—S101	2.4389 (7)	C7—H7	0.9500
Fe1—O1	1.9806 (16)	C9—H9A	0.9900
Fe1—O101	1.9595 (16)	C9—H9B	0.9900
Fe1—N1	2.167 (2)	C9—C10	1.509 (4)
Fe1—N101	2.131 (2)	C10—H10C	0.9800
S1—C8	1.746 (3)	C10—H10D	0.9800
S101—C108	1.752 (2)	C10—H10E	0.9800
O1—C2	1.330 (3)	C101—C102	1.407 (3)
O2—C3	1.387 (3)	C101—C106	1.417 (3)
O2—C9	1.461 (3)	C101—C107	1.448 (3)
O101—C102	1.320 (3)	C102—C103	1.425 (3)
O102—C103	1.381 (3)	C103—C104	1.378 (3)
O102—C109	1.455 (3)	C104—H104	0.9500
N1—N2	1.395 (2)	C104—C105	1.401 (4)
N1—C7	1.301 (3)	C105—H105	0.9500
N2—C8	1.322 (3)	C105—C106	1.377 (4)
N3—H3A	0.840 (17)	C106—H106	0.9500
N3—H3B	0.857 (17)	C107—H107	0.9500
N3—C8	1.352 (3)	C109—H10F	0.9900

N101—N102	1.399 (3)	C109—H10G	0.9900
N101—C107	1.301 (3)	C109—C110	1.515 (4)
N102—C108	1.312 (3)	C110—H11A	0.9800
N103—H10A	0.834 (17)	C110—H11B	0.9800
N103—H10B	0.854 (17)	C110—H11C	0.9800
N103—C108	1.350 (3)	N201—H20A	0.9100
C1—C2	1.417 (3)	N201—H20B	0.9100
C1—C6	1.409 (3)	N201—C201	1.478 (3)
C1—C7	1.451 (3)	N201—C202	1.482 (3)
C2—C3	1.414 (3)	C201—H20C	0.9800
C3—C4	1.382 (3)	C201—H20D	0.9800
C4—H4	0.9500	C201—H20E	0.9800
C4—C5	1.403 (3)	C202—H20F	0.9800
C5—H5	0.9500	C202—H20G	0.9800
C5—C6	1.387 (3)	C202—H20H	0.9800

S1—Fe1—S101	98.98 (2)	C10—C9—H9A	109.6
O1—Fe1—S1	158.48 (5)	C10—C9—H9B	109.6
O1—Fe1—S101	91.30 (5)	C9—C10—H10C	109.5
O1—Fe1—N1	82.17 (7)	C9—C10—H10D	109.5
O1—Fe1—N101	107.31 (7)	C9—C10—H10E	109.5
O101—Fe1—S1	94.31 (5)	H10C—C10—H10D	109.5
O101—Fe1—S101	158.89 (5)	H10C—C10—H10E	109.5
O101—Fe1—O1	81.91 (7)	H10D—C10—H10E	109.5
O101—Fe1—N1	105.56 (7)	C102—C101—C106	119.9 (2)
O101—Fe1—N101	84.03 (7)	C102—C101—C107	121.2 (2)
N1—Fe1—S1	78.45 (5)	C106—C101—C107	118.4 (2)
N1—Fe1—S101	93.18 (5)	O101—C102—C101	123.1 (2)
N101—Fe1—S1	93.26 (5)	O101—C102—C103	118.8 (2)
N101—Fe1—S101	78.93 (5)	C101—C102—C103	118.1 (2)
N101—Fe1—N1	167.63 (7)	O102—C103—C102	114.1 (2)
C8—S1—Fe1	95.87 (8)	C104—C103—O102	125.0 (2)
C108—S101—Fe1	95.71 (8)	C104—C103—C102	120.8 (2)
C2—O1—Fe1	127.41 (14)	C103—C104—H104	119.9
C3—O2—C9	114.40 (18)	C103—C104—C105	120.1 (2)
C102—O101—Fe1	130.25 (16)	C105—C104—H104	119.9
C103—O102—C109	116.38 (18)	C104—C105—H105	119.9
N2—N1—Fe1	120.93 (14)	C106—C105—C104	120.3 (2)
C7—N1—Fe1	124.80 (15)	C106—C105—H105	119.9
C7—N1—N2	114.27 (19)	C101—C106—H106	119.9
C8—N2—N1	113.96 (19)	C105—C106—C101	120.3 (2)
H3A—N3—H3B	127 (3)	C105—C106—H106	119.9
C8—N3—H3A	115.3 (19)	N101—C107—C101	125.9 (2)
C8—N3—H3B	116.1 (18)	N101—C107—H107	117.1
N102—N101—Fe1	122.38 (14)	C101—C107—H107	117.1
C107—N101—Fe1	123.56 (16)	N102—C108—S101	125.65 (18)
C107—N101—N102	113.96 (19)	N102—C108—N103	116.7 (2)
C108—N102—N101	114.09 (19)	N103—C108—S101	117.50 (18)

H10A—N103—H10B	120 (3)	O102—C109—H10F	110.2
C108—N103—H10A	118.5 (19)	O102—C109—H10G	110.2
C108—N103—H10B	116.3 (19)	O102—C109—C110	107.7 (2)
C2—C1—C7	121.2 (2)	H10F—C109—H10G	108.5
C6—C1—C2	119.4 (2)	C110—C109—H10F	110.2
C6—C1—C7	119.1 (2)	C110—C109—H10G	110.2
O1—C2—C1	122.4 (2)	C109—C110—H11A	109.5
O1—C2—C3	118.7 (2)	C109—C110—H11B	109.5
C3—C2—C1	118.8 (2)	C109—C110—H11C	109.5
O2—C3—C2	119.4 (2)	H11A—C110—H11B	109.5
C4—C3—O2	119.6 (2)	H11A—C110—H11C	109.5
C4—C3—C2	120.9 (2)	H11B—C110—H11C	109.5
C3—C4—H4	119.9	H20A—N201—H20B	107.7
C3—C4—C5	120.2 (2)	C201—N201—H20A	108.9
C5—C4—H4	119.9	C201—N201—H20B	108.9
C4—C5—H5	120.0	C201—N201—C202	113.4 (2)
C6—C5—C4	119.9 (2)	C202—N201—H20A	108.9
C6—C5—H5	120.0	C202—N201—H20B	108.9
C1—C6—H6	119.6	N201—C201—H20C	109.5
C5—C6—C1	120.7 (2)	N201—C201—H20D	109.5
C5—C6—H6	119.6	N201—C201—H20E	109.5
N1—C7—C1	125.3 (2)	H20C—C201—H20D	109.5
N1—C7—H7	117.3	H20C—C201—H20E	109.5
C1—C7—H7	117.3	H20D—C201—H20E	109.5
N2—C8—S1	125.75 (17)	N201—C202—H20F	109.5
N2—C8—N3	116.2 (2)	N201—C202—H20G	109.5
N3—C8—S1	118.00 (19)	N201—C202—H20H	109.5
O2—C9—H9A	109.6	H20F—C202—H20G	109.5
O2—C9—H9B	109.6	H20F—C202—H20H	109.5
O2—C9—C10	110.2 (2)	H20G—C202—H20H	109.5
H9A—C9—H9B	108.1		

Fe1—S1—C8—N2	18.8 (2)	C3—O2—C9—C10	−129.0 (2)
Fe1—S1—C8—N3	−163.13 (18)	C3—C4—C5—C6	0.2 (4)
Fe1—S101—C108—N102	17.0 (2)	C4—C5—C6—C1	−0.3 (4)
Fe1—S101—C108—N103	−167.08 (18)	C6—C1—C2—O1	174.2 (2)
Fe1—O1—C2—C1	38.7 (3)	C6—C1—C2—C3	−2.4 (3)
Fe1—O1—C2—C3	−144.75 (18)	C6—C1—C7—N1	172.3 (2)
Fe1—O101—C102—C101	20.9 (3)	C7—N1—N2—C8	165.6 (2)
Fe1—O101—C102—C103	−162.28 (15)	C7—C1—C2—O1	0.7 (4)
Fe1—N1—N2—C8	−14.1 (3)	C7—C1—C2—C3	−175.8 (2)
Fe1—N1—C7—C1	−8.6 (4)	C7—C1—C6—C5	174.9 (2)
Fe1—N101—N102—C108	−8.4 (3)	C9—O2—C3—C2	60.1 (3)
Fe1—N101—C107—C101	−15.1 (3)	C9—O2—C3—C4	−122.8 (3)
O1—C2—C3—O2	2.7 (3)	C101—C102—C103—O102	172.33 (19)
O1—C2—C3—C4	−174.3 (2)	C101—C102—C103—C104	−7.8 (3)
O2—C3—C4—C5	−178.3 (2)	C102—C101—C106—C105	0.1 (3)
O101—C102—C103—O102	−4.6 (3)	C102—C101—C107—N101	−12.6 (4)

O101—C102—C103—C104	175.2 (2)	C102—C103—C104—C105	3.8 (3)
O102—C103—C104—C105	−176.4 (2)	C103—O102—C109—C110	177.88 (19)
N1—N2—C8—S1	−6.2 (3)	C103—C104—C105—C106	2.3 (4)
N1—N2—C8—N3	175.6 (2)	C104—C105—C106—C101	−4.2 (4)
N2—N1—C7—C1	171.7 (2)	C106—C101—C102—O101	−177.3 (2)
N101—N102—C108—S101	−8.5 (3)	C106—C101—C102—C103	5.8 (3)
N101—N102—C108—N103	175.57 (19)	C106—C101—C107—N101	176.1 (2)
N102—N101—C107—C101	168.3 (2)	C107—N101—N102—C108	168.2 (2)
C1—C2—C3—O2	179.4 (2)	C107—C101—C102—O101	11.5 (3)
C1—C2—C3—C4	2.3 (4)	C107—C101—C102—C103	−165.3 (2)
C2—C1—C6—C5	1.4 (4)	C107—C101—C106—C105	171.4 (2)
C2—C1—C7—N1	−14.3 (4)	C109—O102—C103—C102	178.22 (18)
C2—C3—C4—C5	−1.2 (4)	C109—O102—C103—C104	−1.6 (3)

Hydrogen-bond geometry (Å, º)

D—H···*A*	*D*—H	H···*A*	*D*···*A*	*D*—H···*A*
N201—H20*A*···O102	0.91	1.97	2.877 (3)	174
N201—H20*B*···O1	0.91	1.86	2.766 (3)	173